

JOINT ATTENTION-DRIVEN DOMAIN FUSION AND NOISE-TOLERANT LEARNING FOR MULTI-SOURCE DOMAIN ADAPTATION

Tong Xu, Lin Wang, Wu Ning, Chunyan Lyu, Kejun Wang, Chenhui Wang

Harbin Engineering University, The Hong Kong university of Science and Technology
University of California, Los Angeles

ABSTRACT

Multi-source Unsupervised Domain Adaptation (MUDA) transfers knowledge from multiple source domains with labeled data to an unlabeled target domain. Recently, endeavours have been made in establishing connections among different domains to enable feature interaction. However, as these approaches essentially enhance category information, they lack the transfer of the domain-specific information. Moreover, few research has explored the connection between pseudo-label generation and the framework’s learning capabilities, crucial for ensuring robust MUDA. In this paper, we propose a novel framework, which significantly reduces the domain discrepancy and demonstrates new state-of-the-art performance. In particular, we first propose a Contrary Attention-based Domain Merge (CADM) module to enable the interaction among the features so as to achieve the mixture of domain-specific information instead of focusing on the category information. Secondly, to enable the network to correct the pseudo labels during training, we propose an adaptive and reverse cross-entropy loss, which can adaptively impose constraints on the pseudo-label generation process. We conduct experiments on four benchmark datasets, showing that our approach can efficiently fuse all domains for MUDA while showing much better performance than the prior methods.

1 INTRODUCTION

Deep neural networks (DNNs) have achieved excellent performance on various vision tasks under the assumption that training and test data come from the same distribution. However, different scenes have different illumination, viewing angles, and styles, which may cause the domain shift problem (Zhu et al., 2019; Tzeng et al., 2017; Long et al., 2016). This can eventually lead to a significant performance drop on the target task.

Unsupervised Domain Adaptation (UDA) aims at addressing this issue by transferring knowledge from the source domain to the unlabeled target domain (Saenko et al., 2010). Early research has mostly focused on Single-source Unsupervised Domain Adaptation (SUDA), which transfers knowledge from one source domain to the target domain. Accordingly, some methods align the feature distribution among source and target domains (Tzeng et al., 2014; Sun & Saenko, 2016) while some (Tzeng et al., 2017; Saito et al., 2018) learn domain invariants through adversarial learning. Moreover, some methods, *e.g.*, Liang et al. (2020), take the label information as an entry point to maintain the robust training process. However, data is usually collected from multiple domains in the real-world scenario, which arises a more practical task, *i.e.*, Multi-source Unsupervised Domain Adaptation (MUDA) (Duan et al., 2012).

MUDA leverages all of the available data and thus enables performance gains; nonetheless, it introduces a new challenge of reducing domain shift between all source and target domains. For this, some research (Peng et al., 2019; Zhu et al., 2019) builds their methods based on SUDA, aiming to extract common domain-invariant features for all domains. Moreover, some works, *e.g.*, Venkat et al. (2021); Zhou et al. (2021) focus on the classifier’s predictions to achieve domain alignment. Recently, some approaches (Li et al., 2021; Wen et al., 2020) take advantage of the MUDA property to create connections for each domain. These methods attempt to achieve cross-domain consistency

2 RELATED WORK

2.1 UNSUPERVISED DOMAIN ADAPTATION (UDA)

According to the number of source domains, UDA can be divided into Single-source Unsupervised Domain Adaptation (SUDA) and Multi-source Unsupervised Domain Adaptation (MUDA). In SUDA, some methods use the metrics, such as Maximum Mean Discrepancy (Long et al., 2017; Wang et al., 2018), to define and optimize domain shift. Some methods (Sankaranarayanan et al., 2018; Ma et al., 2019) learn the domain-invariant representations through adversarial learning. Other methods are based on the label information. Liang et al. (2020) aligns domains implicitly by constraining the distribution of prediction. Following Liang et al. (2020), Liang et al. (2021) introduces a label shifting strategy as a way to improve the accuracy of low confidence predictions. For MUDA, previous methods eliminate the domain shift while aligning all source domains by constructing multiple source-target pairs, where (Peng et al., 2019; Zhu et al., 2019) are based on the discrepancy metric among different distributions and (Venkat et al., 2021; Ren et al., 2022) are based on the adversarial learning. Some methods (Venkat et al., 2021; Nguyen et al., 2021a; Li et al., 2022; Nguyen et al., 2021b) explore the relation between different classifiers and develop different agreements to achieve domain alignment. Some (Wen et al., 2020; Ahmed et al., 2021) achieve an adaptive transfer by a weighted combination of source domains. Current methods (Wang et al., 2020; Li et al., 2021) mainly construct connections between different domains to enable feature interaction and explore the relation of category information from different domains. Our approach also constructs connections between different domains; however, it mainly transfers domain-specific information to achieve the fusion of all domains.

2.2 ROBUST LOSS FUNCTION UNDER NOISY LABELS

A robust loss function is critical for UDA because the unlabeled target domain requires pseudo labels, which are often noisy. Previous work (Ghosh et al., 2017) demonstrates that some loss functions such as Mean Absolute Error (MAE) are more robust to noisy labels than the commonly used loss functions such as Cross Entropy (CE) loss. (Wang et al., 2019b) proposes the Symmetric Cross Entropy (SCE) combining the Reverse Cross Entropy (RCE) with the CE loss. Moreover, (Wang et al., 2019a) shows that directly adjusting the update process of the loss by the weight variance is effective. Some methods (Venkat et al., 2021; Zhou et al., 2021) mentioned in Section 2.1 focus on exploring a learning strategy to handle prediction values that have high or low confidence levels, respectively. Differently, we design an adaptive loss function for the network to learn robust pseudo-label generation by self-correction.

3 PROBLEM SETTING

For MUDA task, there are N source distributions and one target distribution, which can be denoted as $\{p_{s_j}(x, y)\}_{j=1}^N$ and $\{p_t(x, y)\}$. The labeled source domain images $\{X_{s_j}, Y_{s_j}\}_{j=1}^N$ are obtained from the source distributions, where $\mathcal{X}_{s_j} = \{x_{s_j}^i\}_{i=1}^{|\mathcal{X}_{s_j}|}$ are the images in the source domain j and $\mathcal{Y}_{s_j} = \{y_{s_j}^i\}_{i=1}^{|\mathcal{X}_{s_j}|}$ represents the corresponding ground-truth labels. As for the unlabeled data in the target domain, there are target images $\mathcal{X}_t = \{x_t^i\}_{i=1}^{|\mathcal{X}_t|}$ from target distribution. In this paper, we uniformly set the number of samples in a batch as B , with $b = \frac{B}{N+1}$ for every domain (including the target domain). For a single sample $x_{s_j}^i$, the subscript s_j represents the j -th source domain, while the superscript i indicates that it is the i -th sample in that domain.

4 PROPOSED METHOD

4.1 OVERALL FRAMEWORK

The general MUDA pipeline consists of two phases: 1) pre-training on the source domain; 2) training when transferring to the target domain. The base structure of the model consists of a feature extractor $F(\cdot)$ and a classifier $C(\cdot)$. In the pre-training phase, we use the source domain data $\{X_{s_j}, Y_{s_j}\}_{j=1}^N$

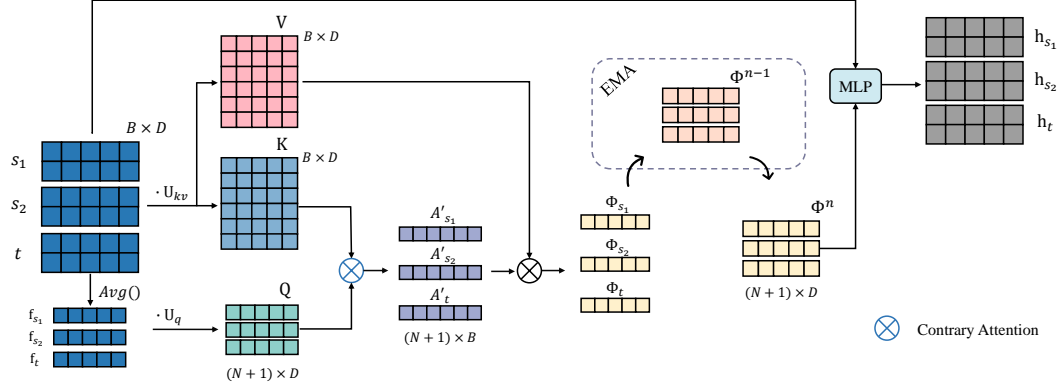


Figure 2: CADM review: Features from different domains are fused by CADM. For simplicity, we set N , B , and D as 2, 6, and 5, respectively. Domain prototypes are mapped to \mathbf{Q} , while all features are mapped to \mathbf{K} and \mathbf{V} . The domain style centroids are obtained by the contrary attention map A' and \mathbf{V} , which is then updated by EMA. Finally, the fused feature \mathbf{h} is obtained by MLP.

for training to obtain the pre-trained $F(\cdot)$ and $C(\cdot)$. In the training phase for the target domain, we firstly feed the source domain data $\{X_{s_j}, Y_{s_j}\}_{j=1}^N$ and target domain data X_t into $F(\cdot)$ to get the features \mathbf{f} , and perform the feature fusion by CADM to get the fused feature \mathbf{h} . Then, we use the fused features of the target domain for the pseudo-label generation and feed the fused features of all domains into $C(\cdot)$ to get prediction values. Finally, we compute the loss based on the labels. Since source training is general, training in this paper typically refers to target domain training.

4.2 CONTRARY ATTENTION-BASED DOMAIN MERGE MODULE

The proposed CADM enables the passing of domain-specific information to achieve the deep fusion of all domains. *The main idea is to allow features to receive information from other domains in an adaptive manner based on their relevance.* The specific structure is shown in Fig. 2. First, we use each domain to query the correlation with other domains. Specifically, samples are first mapped into the latent space via F to obtain feature \mathbf{f} . Then, we define the mean embedding of features in a domain as the domain prototype:

$$\mathbf{f}_g = \frac{1}{b} \sum_{i=1}^b \mathbf{f}_g^i \quad (1)$$

where \mathbf{f}_g represents the domain prototype of domain g and is then used to compute correlations with features in other domains as shown below:

$$\mathbf{Q} = [\mathbf{f}_{s_1} \dots \mathbf{f}_{s_N}, \mathbf{f}_t] \mathbf{U}_q \quad \mathbf{U}_q \in \mathbb{R}^{D \times D} \quad (2)$$

$$[\mathbf{K}, \mathbf{V}] = [\mathbf{f}_{s_1}^1 \dots \mathbf{f}_{s_2}^1 \dots \mathbf{f}_t^b] \mathbf{U}_{kv} \quad \mathbf{U}_{kv} \in \mathbb{R}^{D \times 2D} \quad (3)$$

$$A_g = \text{Softmax} \left(\frac{\mathbf{q}_g \cdot \mathbf{K}^T}{\sqrt{D}} \right) \quad A_g \in \mathbb{R}^{1 \times B} \quad (4)$$

where \mathbf{U}_q and \mathbf{U}_{kv} are learnable projection matrices that are used to map the domain prototype and all features to the new space respectively. We use the cross-attention mechanism (Vaswani et al., 2017; Dosovitskiy et al., 2020) to model the correlation because of its powerful ability to capture dependencies. In Eq. 4, \mathbf{q}_g is the query feature of the domain g , and A_g is the obtained attention map through cross attention.

With the above formula, more emphasis is given to features that are more semantically close to the domain prototype, i.e., domain styles similar to g . However, such emphasis primarily strengthens the original domain style information of g and does not help eliminate the domain shift. Instead, we take a different perspective, forcing the network to focus on features that are semantically distinct from the domain prototypes, which often have different domain-specific information. Specifically, we ‘reverse’ the obtained A_g to generate a new attention map, which we refer to as the contrary

attention map:

$$A'_g = \frac{\mathbf{1} - A_g}{\text{sum}(\mathbf{1} - A_g)} \quad A'_g \in \mathbb{R}^{1 \times B} \quad (5)$$

where $\mathbf{1}$ is an all-one vector. The A'_g thus obtained can achieve the opposite effect of the previous A_g , where those features that are more different from the domain g in terms of domain-specific information are assigned higher weights.

Subsequently, we use A'_g to perform the feature fusion for domain g , which allows the merging of information from features according to their degree of dissimilarity with domain g .

$$\begin{aligned} \Phi_g &= A'_g \cdot \mathbf{V} \\ &= \sum_{\hat{g} \in \mathcal{G}} \sum_{i=1}^b a'_{g\hat{g}i} \mathbf{v}_g^i \end{aligned} \quad (6)$$

where $a'_{g\hat{g}i}$ represents the contrary attention weight between the prototype of g and the i -th feature in \hat{g} . Φ_g is obtained by weighting features from different domains and summing them according to their discrepancies from g . Given its greater emphasis on the merging of knowledge with distinct styles, we call Φ_g the domain style centroid with respect to g . In addition, to guarantee the robustness of Φ_g , we use exponential moving averages (EMA) to maintain it:

$$(\bar{\Phi}_g)^n = (1 - \alpha)(\bar{\Phi}_g)^{n-1} + \alpha(\Phi_g)^n \quad (7)$$

where n denotes the n -th mini-batch. The recorded $\bar{\Phi}_g$ will be used in the inference phase.

Finally, we integrate the domain style centroid $\bar{\Phi}_g$ into the original features. A fundamental MLP is used to simulate this process:

$$\mathbf{h}_g^i = \text{MLP}([\mathbf{f}_g^i, \bar{\Phi}_g]) \quad (8)$$

where \mathbf{h}_g^i is the fused feature and $\bar{\Phi}_g$ is integrated into every feature in g , thus creating the overall movement of domain. Through the process described above, the original features achieve the merging of different domain-specific information by integrating the domain style centroid. Meanwhile, to maintain a well-defined decision boundary during such domain fusion, we use a metric-based loss (Wen et al., 2016) to optimize the intra-class distance. It allows samples from the same categories to be close to each other and shrink around the class center.

$$\mathcal{L}_{Cr} = \sum_{g \in \mathcal{G}} \sum_{i=1}^b \|\mathbf{h}_g^i - \mu_{y_g^i}\|_2^2 \quad (9)$$

where y_g^i is the label of \mathbf{h}_g^i and $\mu_{y_g^i} \in \mathbb{R}^{1 \times D}$ denotes the y_g^i -th class center. For the robustness of class center, we maintain a memory \mathbf{M} to store features at the class level and update them batch by batch during training, which is widely applied in UDA (Saito et al., 2020). The class-level features can be regarded as the class center, and we then apply them in the computation of \mathcal{L}_{Cr} . Specifically, we traverse all the datasets to extract features and obtain different class centers before the training process. In the target domain, we use the classification result as the category since there is no ground-truth label:

$$\mu_k = \text{Avg} \left(\sum_{j=1}^N \sum_{x_i \in \mathcal{X}_{s_j}}^{y_i=k} \mathbf{h}_{s_j}^i + \sum_{x_i \in \mathcal{X}_t}^{\arg \max_j p_j(x_i)=k} \mathbf{h}_t^i \right) \quad (10)$$

where $p_j(x)$ represents the confidence level of predicting x as the j -th class. Then after each back-propagation step, we update the memory \mathbf{M} with the following rule:

$$\mu_k^{new} = (1 - \beta)\mu_k^{old} + \beta \mathbf{h} \quad (11)$$

where k is the label of \mathbf{h} and μ_k is the k -th class center in \mathbf{M} . Under the supervision of \mathcal{L}_{Cr} , the features are able to maintain intra-class compactness in domain movement.

Overall, through CADM, we establish connections among domains and enable the deep fusion of different domains. Eventually, with the \mathcal{L}_{Cr} , the model is able to reach a tradeoff between domain merging and a well-defined decision boundary.

4.3 ADAPTIVE AND REVERSE CROSS ENTROPY LOSS

General UDA methods use the K-means-like algorithm to generate pseudo labels for the entire unlabeled target dataset. However, it has been observed that the pseudo labels generated in this way are often misassigned due to the lack of constraints, which introduces noise and impairs performance. To address this issue, we creatively propose to assign gradients to the generation process of pseudo labels and constrain it with a well-designed rule, so that the network can optimize both the prediction values and pseudo labels simultaneously. To begin, we expect to obtain the pseudo labels with gradient flow. Since the dynamically updated memory M is introduced in Section 4.2, we can obtain both soft labels and hard labels by computing the distance between features and the class-level features in M in every batch:

$$q(y = k|x) = \frac{e^{\mathbf{h} \cdot \mu_k^T}}{\sum_{j=1}^K e^{\mathbf{h} \cdot \mu_j^T}} \quad (12)$$

$$\hat{y} = \arg \max_k q(y = k|x) \quad (13)$$

where $q(y|x)$ is the soft label and \hat{y} is the hard label. The soft label thus obtained makes the gradient backpropagation possible and can be supervised by a designed loss function. Furthermore, due to the noise in pseudo labels, this generation may lead to error accumulation and is therefore required to be constrained. Previous experimental observations (Venkat et al., 2021; Wang et al., 2019b) demonstrate that the trained classifier has abundant information, which is key to preventing the model from collapsing in the unlabeled target domain. Therefore, based on the prediction values of the classifier, we establish constraints on the pseudo-label generation by a reverse cross entropy loss:

$$\ell_{rce} = \sum_{k=1}^K p_k(x) \log q(y = k|x) \quad (14)$$

where $p_k(x)$ represents the confidence level of predicting x as the k -th class. Such a constraint prevents the overly aggressive pseudo-label generation and error accumulation. However, it is unfair to apply the same rule to those pseudo labels that tend to be accurate. An ideal situation is that the constraints can be adaptively adjusted to correspond to different pseudo labels. Since pseudo label essentially arises from the feature extracted by the network, its accuracy is closely related to the ability of the network to distinguish this sample. Liang et al. (2021) demonstrates that when the model has a good distinguishing ability for one sample, the corresponding prediction values should be close to the one-hot vector. Inspired by it, we design an adaptive and reverse cross entropy loss:

$$\delta_j(x, \hat{y}) = \frac{p_j(x)}{1 - p_{\hat{y}}(x)} \quad (15)$$

$$\ell_{arce}(x, \hat{y}) = \frac{\ell_{rce}}{\exp \left(\left(- \sum_{j \neq \hat{y}} \delta_j(x, \hat{y}) \log \delta_j(x, \hat{y}) \right) / \tau \right)} \quad (16)$$

$$\mathcal{L}_{AR-CE} = \sum_i^B \ell_{arce}(x_i, \hat{y}_i) \quad (17)$$

where \hat{y} is the generated hard label of the target domain sample x . $\delta_j(x, \hat{y})$ in Eq. 16 is the distribution of the prediction values except for the prediction values of the class \hat{y} (hard label). The low entropy of this distribution represents the existence of a high prediction value except for the class \hat{y} , which is not in accordance with the previously mentioned one-hot vector assumption, and therefore the network has a relatively weak distinguishing ability for this sample. Similarly, a high entropy of this distribution represents the network tends to make the correct prediction and has a good distinguishing ability for this sample. As a result, we use the entropy of this distribution to implement an adaptive adjustment mechanism for the constraints, as shown in Eq. 16. The exponential form and τ are used to amplify its effect. Since \mathcal{L}_{AR-CE} aims to focus on the optimization of pseudo label, we freeze the gradient of the prediction values in Eq. 14. The backpropagation of \mathcal{L}_{AR-CE} can eventually enable the optimization of pseudo-label generation.

Furthermore, the usual cross entropy loss is denoted as follows:

$$\mathcal{L}_{CE} = -\frac{1}{B} \sum_{i=1}^B \log p_{y_i}(x_i) \quad (18)$$

where y_i is the ground-truth label for source domain sample and is the hard pseudo label \hat{y}_i obtained by Eq. 13 when x_i is in the target domain.

Ultimately, the loss function for the entire framework can be represented as follows:

$$\mathcal{L} = \mathcal{L}_{CE} + \mathcal{L}_{Cr} + \mathcal{L}_{AR-CE} \quad (19)$$

where \mathcal{L}_{CE} is the normal cross entropy loss, \mathcal{L}_{Cr} is for feature fusion, \mathcal{L}_{AR-CE} is used for noise tolerant learning, and the latter one item acts only on the target domain.

5 EXPERIMENTS

5.1 DATASETS AND IMPLEMENTATION

Office-31 (Saenko et al., 2010) is a fundamental domain adaptation dataset comprised of three separate domains: Amazon (A), Webcam (W), and DSLR (D). Office-Caltech (Gong et al., 2012) has an additional domain Caltech-256 (C) than Office-31. Office-Home (Venkateswara et al., 2017) is a medium-size dataset which contains four domains: Art (Ar), Clipart (Cl), Product (Pr), and Real-World (Rw). DomainNet (Peng et al., 2019) is the largest dataset available for MUDA. It contains 6 different domains: Clipart (Clp), Infograph (Inf), Painting (Pnt), Quickdraw (Qdr), Real (Rel), and Sketch (Skt).

For a comparison with our method, we introduce the SoTA methods on MUDA, including DCTN (Xu et al., 2018), M³SDA (Peng et al., 2019), MFSAN (Zhu et al., 2019), MDDA (Zhao et al., 2020), DARN (Wen et al., 2020), Ltc-MSDA (Wang et al., 2020), SHOT++ (Liang et al., 2021), SImpAI (Venkat et al., 2021), T-SVDNet (Li et al., 2021), CMSS (Ahmed et al., 2021), DECISION (Ahmed et al., 2021), DAEL (Zhou et al., 2021), PTMDA (Ren et al., 2022) and DINE (Liang et al., 2022).

For Office-31, Office-Caltech and Office-Home, we use an Imagenet (Deng et al., 2009) pre-trained ResNet-50 (He et al., 2016) as the feature extractor. As for the DomainNet, we use ResNet-101 instead. In addition, a bottleneck layer (consists of two fully-connected layers) is used as the classifier. We use the Adam optimizer with a learning rate of 1×10^{-6} and a weight decay of 5×10^{-4} . We set the learning rate of extractor to ten times that of the classifier. The hyperparameters α and β are set to 0.05 and 0.005, respectively. All the framework is based on the Pytorch (Paszke et al., 2019).

5.2 RESULTS

We compare the ADNT with different approaches on four datasets, and the results are shown in the following tables. Note that the one pointed by the arrow is the target domain and the others are the source domains. Experimenting on the Office-31 dataset, we achieve optimal results in all scenarios, except for transferring W and D to A. On the Office-Caltech dataset, our method not only outperforms all current approaches, but also achieves an impressive 100% accuracy on the task of transferring to W and to D. In terms of the medium-sized Office-Home dataset, our proposed ADNT is the best performer and has a significant lead among the ResNet-50-based method. Compared with the ResNet-101-based methods (DINE and SImpAI₁₀₁), our approach achieves leading performance with fewer parameters and a simpler model structure. As shown in Table 4, ADNT also demonstrates its strength on the largest and most challenging dataset. The total result outperforms the current optimal method by 2.3%, which is highly impressive on DomainNet.

5.3 ABLATION STUDY

To verify the effectiveness of the proposed components, we conduct ablation experiments on the Office-Home dataset, as shown in Table 5. In order to determine whether the attention-driven module actually achieves domain fusion, we conduct experiments with only the domain fusion without

Table 1: Classification accuracies (%) on Office-31 dataset, “*” indicates that the method is based on ResNet-101.

Method	A,W →D	A,D →W	D,W →A	Avg
MDDA	99.2	97.1	56.2	84.2
LtC-MSDA	99.6	97.2	56.9	84.6
DCTN	99.3	98.2	64.2	87.2
MFSAN	99.5	98.5	72.7	90.2
SImpAl ₅₀	99.2	97.4	70.6	89.0
DECISION	99.6	98.4	75.4	91.1
DINE*	99.2	98.4	76.8	91.5
PTMDA	100	99.6	75.4	91.7
ADNT (Ours)	100	99.6	74.4	91.3

Table 2: Classification accuracies (%) on Office-Caltech dataset. “*” indicates that the method is based on ResNet-101.

Method	A,C,D →W	A,C,W →D	A,W,D →C	C,D,W →A	Avg
DCTN	99.4	99.0	90.2	92.7	95.3
M ³ SDA	99.4	99.2	91.5	94.1	96.1
SImpAl ₅₀	99.3	99.8	92.2	95.3	96.7
CMSS	99.3	99.6	96.6	93.7	97.2
SHOT++	100	99.4	96.5	96.2	98.0
DECISION	99.6	100	95.9	95.9	98.0
DINE*	98.9	98.5	95.2	95.9	97.1
PTMDA	100	100	96.5	96.7	98.3
ADNT (Ours)	100	100	97.6	96.3	98.5

Table 3: Classification accuracies (%) on Office-Home dataset, “*” indicates that the method is based on ResNet-101.

Method	Cl,Pr,Rw →Ar	Ar,Pr,Rw →Cl	Ar,Cl,Rw →Pr	Ar,Cl,Pr →Rw	Avg
MFSAN	72.1	62.0	80.3	81.8	74.1
SImpAl ₅₀	70.8	56.3	80.2	81.5	72.2
SImpAl ₁₀₁ *	73.4	62.4	81.0	82.7	74.8
DARN	70.0	68.4	82.7	83.9	76.3
SHOT++	73.1	61.3	84.3	84.0	75.7
DECISION	74.5	59.4	84.4	83.6	75.5
DINE*	74.8	64.1	85.0	84.6	77.1
ADNT (Ours)	73.8	66.5	85.1	83.3	77.2

\mathcal{L}_{Cr} , which is shown as ‘+ CADM (w/o \mathcal{L}_{Cr})’ in the table. Additionally, due to the fact that our proposed contrary attention differs from general attention by paying attention to the fusion of domain-specific information, a comparison with general attention can evaluate the viability of our strategy. Therefore, we replace the contrary attention map in the proposed CADM with a general attention map, i.e., without Eq. 5. The result of general attention is shown as ‘+ ADM’ in Table 5. The significant performance improvement powerfully demonstrates the effectiveness of our proposed CADM.

We also use t-sne (Van der Maaten & Hinton, 2008) to visualize the results with and without CADM, as shown in Fig. 3. We can observe that with the designed CADM, the different distributions are mixed with each other, achieving a higher degree of fusion. Meanwhile, the decision boundaries of different categories are more distinct. Table 5 verifies the effectiveness of our AR-CE loss. Moreover, the accuracy of the pseudo labels can reflect the effectiveness and stability of the pseudo-label generation. Therefore, we compare the average accuracy of pseudo labels generated with and without AR-CE loss on Office-31, Office-Caltech and Office-Home, which is shown in Fig. 4. Specifically, we calculate the mean accuracy of the final five epochs during training. It can be seen that after the introduction of the AR-CE loss, the model can derive noisy labels through self-correction and achieve the high accuracy of pseudo labels. Due to the space limit, additional analytical experiments, including the visualization of the training process and analysis of hyperparameters, can be found in the appendix.

6 CONCLUSION

This paper proposes the ADNT, a framework that combines the domain fusion module and robust loss function under noisy labels. Firstly, We construct a contrary attention-based domain merge module, which can achieve a mixture of different domain-specific information and thus fuse features from different domains. In addition, we design a robust loss function to avoid the error accumula-

Table 4: Classification accuracies (%) on DomainNet dataset.

Methods	→ Clp	→ Inf	→ Pnt	→ Qdr	→ Rel	→ Skt	Avg
DCTN	48.6±0.70	23.5±0.60	48.8±0.60	7.2±0.50	53.5±0.60	47.3±0.50	38.2
M ³ SDA	58.6±0.53	26.0±0.89	52.3±0.55	6.3±0.58	62.7±0.51	49.5±0.76	42.6
MDDA	59.4±0.60	23.8±0.80	53.2±0.60	12.5±0.60	61.8±0.50	48.6±0.80	43.2
CMSS	64.2±0.20	28.0±0.20	53.6±0.40	16.0±0.10	63.4±0.20	53.8±0.40	46.5
T-SVDNet	66.1±0.4	25.0±0.8	54.3±0.7	16.5±0.9	65.4±0.5	54.6±0.6	47.0
LtC-MSDA	63.1±0.5	28.7±0.7	56.1±0.5	16.3±0.5	66.1±0.6	53.8±0.6	47.4
DAEL	70.8±0.14	26.5±0.13	57.4±0.28	12.2±0.70	65.0±0.23	60.6±0.25	48.7
PTMDA	66.0±0.3	28.5±0.2	58.4±0.4	13.0±0.5	63.0±0.24	54.1±0.3	47.2
ADNT (ours)	69.0±0.38	28.2±0.41	60.5±0.45	16.3±0.66	68.7±0.63	63.5±0.69	51.0

Table 5: Classification accuracies (%) of ablation study on Office-Home dataset.

Method	Cl,Pr,Rw	Ar,Pr,Rw	Ar,Cl,Rw	Ar,Cl,Pr	Avg
	→Ar	→Cl	→Pr	→Rw	
Baseline	67.1	56.6	78.6	77.0	69.8
+ \mathcal{L}_{AR-CE}	69.2	63.1	81.2	78.6	73.0
+ ADM	69.7	60.2	81.3	79.5	72.7
+ CADM (w/o \mathcal{L}_{Cr})	72.3	62.2	83.1	83.1	75.2
+ CADM (w/ \mathcal{L}_{Cr})	73.1	64.2	84.3	83.7	76.3
+ CADM (w/ \mathcal{L}_{Cr}) + \mathcal{L}_{AR-CE}	73.8	66.5	85.1	83.3	77.2

tion of pseudo-label generation. Substantial experiments on four datasets have shown the superior performance of ADNT, which strongly demonstrates the effectiveness of our approach.

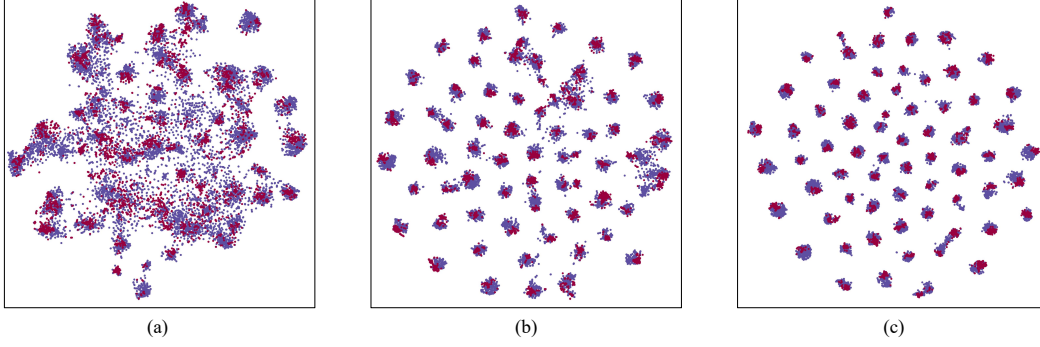


Figure 3: t-sne: The results of feature visualization on the Office-Home dataset, while performing Ar, Cl, Rw to Pr. (a) (b) and (c) represent the result of Source-only, CADM without \mathcal{L}_{Cr} and CADM with \mathcal{L}_{Cr} respectively. All source domains are represented in red, while target domain is represented in blue.

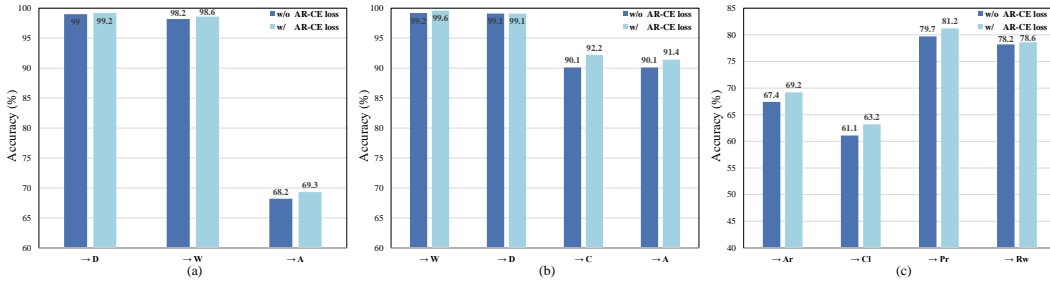


Figure 4: Mean accuracies (%) of pseudo labels on three datasets. (a), (b), (c) represent the result on Office-31, Office-Caltech and Office-Home respectively.

REFERENCES

- Sk Miraj Ahmed, Dripta S Raychaudhuri, Sujoy Paul, Samet Oymak, and Amit K Roy-Chowdhury. Unsupervised multi-source domain adaptation without access to source data. In *Proceedings of the IEEE/CVF Conference on Computer Vision and Pattern Recognition*, pp. 10103–10112, 2021.
- Jia Deng, Wei Dong, Richard Socher, Li-Jia Li, Kai Li, and Li Fei-Fei. Imagenet: A large-scale hierarchical image database. In *2009 IEEE conference on computer vision and pattern recognition*, pp. 248–255. Ieee, 2009.
- Alexey Dosovitskiy, Lucas Beyer, Alexander Kolesnikov, Dirk Weissenborn, Xiaohua Zhai, Thomas Unterthiner, Mostafa Dehghani, Matthias Minderer, Georg Heigold, Sylvain Gelly, et al. An image is worth 16x16 words: Transformers for image recognition at scale. *arXiv preprint arXiv:2010.11929*, 2020.
- Lixin Duan, Dong Xu, and Ivor Wai-Hung Tsang. Domain adaptation from multiple sources: A domain-dependent regularization approach. *IEEE Transactions on neural networks and learning systems*, 23(3):504–518, 2012.
- Aritra Ghosh, Himanshu Kumar, and PS Sastry. Robust loss functions under label noise for deep neural networks. In *Proceedings of the AAAI Conference on Artificial Intelligence*, volume 31, 2017.
- Boqing Gong, Yuan Shi, Fei Sha, and Kristen Grauman. Geodesic flow kernel for unsupervised domain adaptation. In *2012 IEEE conference on computer vision and pattern recognition*, pp. 2066–2073. IEEE, 2012.
- Kaiming He, Xiangyu Zhang, Shaoqing Ren, and Jian Sun. Deep residual learning for image recognition. In *Proceedings of the IEEE conference on computer vision and pattern recognition*, pp. 770–778, 2016.
- Keqiuyin Li, Jie Lu, Hua Zuo, and Guangquan Zhang. Dynamic classifier alignment for unsupervised multi-source domain adaptation. *IEEE Transactions on Knowledge and Data Engineering*, 2022.
- Ruihuang Li, Xu Jia, Jianzhong He, Shuaijun Chen, and Qinghua Hu. T-svdnet: Exploring high-order prototypical correlations for multi-source domain adaptation. In *Proceedings of the IEEE/CVF International Conference on Computer Vision*, pp. 9991–10000, 2021.
- Jian Liang, Dapeng Hu, and Jiashi Feng. Do we really need to access the source data? source hypothesis transfer for unsupervised domain adaptation. In *International Conference on Machine Learning*, pp. 6028–6039. PMLR, 2020.
- Jian Liang, Dapeng Hu, Yunbo Wang, Ran He, and Jiashi Feng. Source data-absent unsupervised domain adaptation through hypothesis transfer and labeling transfer. *IEEE Transactions on Pattern Analysis and Machine Intelligence*, 2021.
- Jian Liang, Dapeng Hu, Jiashi Feng, and Ran He. Dine: Domain adaptation from single and multiple black-box predictors. In *Proceedings of the IEEE/CVF Conference on Computer Vision and Pattern Recognition*, pp. 8003–8013, 2022.
- Mingsheng Long, Han Zhu, Jianmin Wang, and Michael I Jordan. Unsupervised domain adaptation with residual transfer networks. *arXiv preprint arXiv:1602.04433*, 2016.
- Mingsheng Long, Han Zhu, Jianmin Wang, and Michael I Jordan. Deep transfer learning with joint adaptation networks. In *International conference on machine learning*, pp. 2208–2217. PMLR, 2017.
- Xinhong Ma, Tianzhu Zhang, and Changsheng Xu. Gcan: Graph convolutional adversarial network for unsupervised domain adaptation. In *Proceedings of the IEEE/CVF Conference on Computer Vision and Pattern Recognition*, pp. 8266–8276, 2019.
- Tuan Nguyen, Trung Le, He Zhao, Quan Hung Tran, Truyen Nguyen, and Dinh Phung. Most: Multi-source domain adaptation via optimal transport for student-teacher learning. In *Uncertainty in Artificial Intelligence*, pp. 225–235. PMLR, 2021a.

- Van-Anh Nguyen, Tuan Nguyen, Trung Le, Quan Hung Tran, and Dinh Phung. Stem: An approach to multi-source domain adaptation with guarantees. In *Proceedings of the IEEE/CVF International Conference on Computer Vision*, pp. 9352–9363, 2021b.
- Adam Paszke, Sam Gross, Francisco Massa, Adam Lerer, James Bradbury, Gregory Chanan, Trevor Killeen, Zeming Lin, Natalia Gimelshein, Luca Antiga, Alban Desmaison, Andreas Kopf, Edward Yang, Zachary DeVito, Martin Raison, Alykhan Tejani, Sasank Chilamkurthy, Benoit Steiner, Lu Fang, Junjie Bai, and Soumith Chintala. Pytorch: An imperative style, high-performance deep learning library. In H. Wallach, H. Larochelle, A. Beygelzimer, F. d'Alché-Buc, E. Fox, and R. Garnett (eds.), *Advances in Neural Information Processing Systems*, volume 32. Curran Associates, Inc., 2019. URL <https://proceedings.neurips.cc/paper/2019/file/bdbca288fee7f92f2bfa9f7012727740-Paper.pdf>.
- Xingchao Peng, Qinxun Bai, Xide Xia, Zijun Huang, Kate Saenko, and Bo Wang. Moment matching for multi-source domain adaptation. In *Proceedings of the IEEE/CVF International Conference on Computer Vision*, pp. 1406–1415, 2019.
- Chuan-Xian Ren, Yong-Hui Liu, Xi-Wen Zhang, and Ke-Kun Huang. Multi-source unsupervised domain adaptation via pseudo target domain. *IEEE Transactions on Image Processing*, 31:2122–2135, 2022.
- Kate Saenko, Brian Kulis, Mario Fritz, and Trevor Darrell. Adapting visual category models to new domains. In *European conference on computer vision*, pp. 213–226. Springer, 2010.
- Kuniaki Saito, Kohei Watanabe, Yoshitaka Ushiku, and Tatsuya Harada. Maximum classifier discrepancy for unsupervised domain adaptation. In *Proceedings of the IEEE conference on computer vision and pattern recognition*, pp. 3723–3732, 2018.
- Kuniaki Saito, Donghyun Kim, Stan Sclaroff, and Kate Saenko. Universal domain adaptation through self supervision. *Advances in neural information processing systems*, 33:16282–16292, 2020.
- Swami Sankaranarayanan, Yogesh Balaji, Carlos D Castillo, and Rama Chellappa. Generate to adapt: Aligning domains using generative adversarial networks. In *Proceedings of the IEEE Conference on Computer Vision and Pattern Recognition*, pp. 8503–8512, 2018.
- Baochen Sun and Kate Saenko. Deep coral: Correlation alignment for deep domain adaptation. In *European conference on computer vision*, pp. 443–450. Springer, 2016.
- Eric Tzeng, Judy Hoffman, Ning Zhang, Kate Saenko, and Trevor Darrell. Deep domain confusion: Maximizing for domain invariance. *arXiv preprint arXiv:1412.3474*, 2014.
- Eric Tzeng, Judy Hoffman, Kate Saenko, and Trevor Darrell. Adversarial discriminative domain adaptation. In *Proceedings of the IEEE conference on computer vision and pattern recognition*, pp. 7167–7176, 2017.
- Laurens Van der Maaten and Geoffrey Hinton. Visualizing data using t-sne. *Journal of machine learning research*, 9(11), 2008.
- Ashish Vaswani, Noam Shazeer, Niki Parmar, Jakob Uszkoreit, Llion Jones, Aidan N Gomez, Łukasz Kaiser, and Illia Polosukhin. Attention is all you need. In *Advances in neural information processing systems*, pp. 5998–6008, 2017.
- Naveen Venkat, Jogendra Nath Kundu, Durgesh Kumar Singh, Ambareesh Revanur, and R Venkatesh Babu. Your classifier can secretly suffice multi-source domain adaptation. *arXiv preprint arXiv:2103.11169*, 2021.
- Hemanth Venkateswara, Jose Eusebio, Shayok Chakraborty, and Sethuraman Panchanathan. Deep hashing network for unsupervised domain adaptation. In *Proceedings of the IEEE conference on computer vision and pattern recognition*, pp. 5018–5027, 2017.
- Hang Wang, Minghao Xu, Bingbing Ni, and Wenjun Zhang. Learning to combine: Knowledge aggregation for multi-source domain adaptation. In *European Conference on Computer Vision*, pp. 727–744. Springer, 2020.

- Jindong Wang, Wenjie Feng, Yiqiang Chen, Han Yu, Meiyu Huang, and Philip S Yu. Visual domain adaptation with manifold embedded distribution alignment. In *Proceedings of the 26th ACM international conference on Multimedia*, pp. 402–410, 2018.
- Xinshao Wang, Yang Hua, Elyor Kodirov, and Neil M Robertson. Imae for noise-robust learning: Mean absolute error does not treat examples equally and gradient magnitude’s variance matters. *arXiv preprint arXiv:1903.12141*, 2019a.
- Yisen Wang, Xingjun Ma, Zaiyi Chen, Yuan Luo, Jinfeng Yi, and James Bailey. Symmetric cross entropy for robust learning with noisy labels. In *Proceedings of the IEEE/CVF International Conference on Computer Vision*, pp. 322–330, 2019b.
- Junfeng Wen, Russell Greiner, and Dale Schuurmans. Domain aggregation networks for multi-source domain adaptation. In *International Conference on Machine Learning*, pp. 10214–10224. PMLR, 2020.
- Yandong Wen, Kaipeng Zhang, Zhifeng Li, and Yu Qiao. A discriminative feature learning approach for deep face recognition. In *European conference on computer vision*, pp. 499–515. Springer, 2016.
- Ruijia Xu, Ziliang Chen, Wangmeng Zuo, Junjie Yan, and Liang Lin. Deep cocktail network: Multi-source unsupervised domain adaptation with category shift. In *Proceedings of the IEEE Conference on Computer Vision and Pattern Recognition*, pp. 3964–3973, 2018.
- Sicheng Zhao, Guangzhi Wang, Shanghang Zhang, Yang Gu, Yaxian Li, Zhichao Song, Pengfei Xu, Runbo Hu, Hua Chai, and Kurt Keutzer. Multi-source distilling domain adaptation. In *Proceedings of the AAAI Conference on Artificial Intelligence*, volume 34, pp. 12975–12983, 2020.
- Kaiyang Zhou, Yongxin Yang, Yu Qiao, and Tao Xiang. Domain adaptive ensemble learning. *IEEE Transactions on Image Processing*, 30:8008–8018, 2021.
- Yongchun Zhu, Fuzhen Zhuang, and Deqing Wang. Aligning domain-specific distribution and classifier for cross-domain classification from multiple sources. In *Proceedings of the AAAI Conference on Artificial Intelligence*, volume 33, pp. 5989–5996, 2019.

A APPENDIX

A.0.1 VISUALIZATION OF THE TRAINING

In our proposed CADM, the weight value in A' actually reflects the correlation between domains (Here, we use the domain to refer to the features in the domain). Therefore, We estimate the state between domains by analyzing A' . In this paper, we expect the following domain relationship: Initially, they should have very different styles, and the weights in A' will be quite uncertain. Then, as the optimization of the model parameters, different domains will gradually be mixed. Finally, all domains should have a consistent style and maintain a balanced relationship. Therefore, the merging of all domains together means that there should be little difference among the final correlation coefficients in A' . So we calculate the standard deviation of A' during the training.

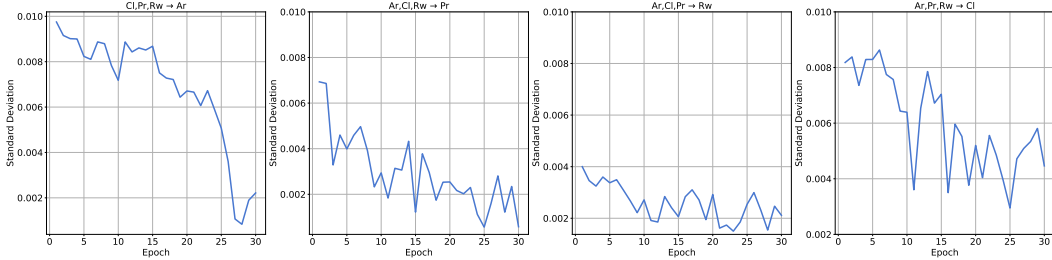


Figure 5: The standard deviation of A' on the Office-Home dataset.

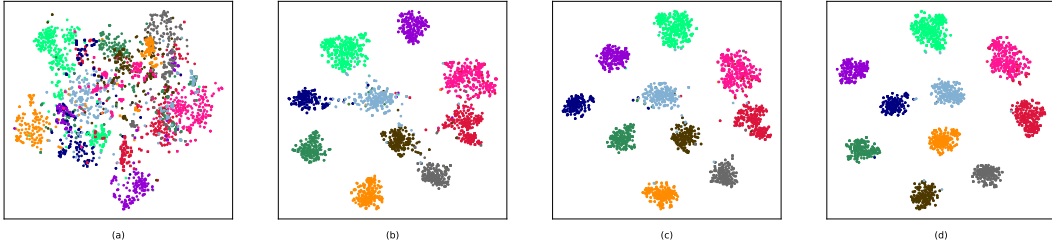


Figure 6: Visualization of the feature distribution during the training process in the transfer task Ar, Cl, Rw to Pr. (a), (b), (c) and (d) represent the epoch 1, 10, 20 and 30, respectively. To provide a clearer illustration, we select features from the first ten classes of each domain, with different color representing different class. Solid circles represent all source domains, while the squares represent target domains. Best viewed enlarged.

As shown in the Fig. 5, during the training process, the standard deviation gradually becomes smaller and eventually tends to be stable, which indicates that the features from different domains are distributed in the space with a uniform state.

However, the above results alone do not demonstrate that features from different domains are deeply fused because the previous effect in Fig. 5 can also be achieved if features are sufficiently separated from each other. Consequently, we map the fused features \mathbf{h} into the low-dimensional space and visualize the distribution during the training process, divided by different domains and categories. As shown in Fig. 6, at the start of training, the fused features are distributed haphazardly in space, and the network does not have capacity to process them. Then, different domains gradually move toward each other and merge together as the updating of model parameters. Finally, the features of the same category become more compact while preserving domain fusion. This powerfully demonstrates that through CADM, different domains embrace each other and achieve deep fusion. We make the model learn how to handle the fused features and show its excellent results.

A.1 PARAMETER ANALYSIS

In addition, exponential moving average (EMA) is used in the experiments to maintain the domain style centers and class-level features, so the selection of hyperparameters α and β requires additional analysis and verification. Therefore, we perform an experimental comparison of their values and present them in Fig. 7.

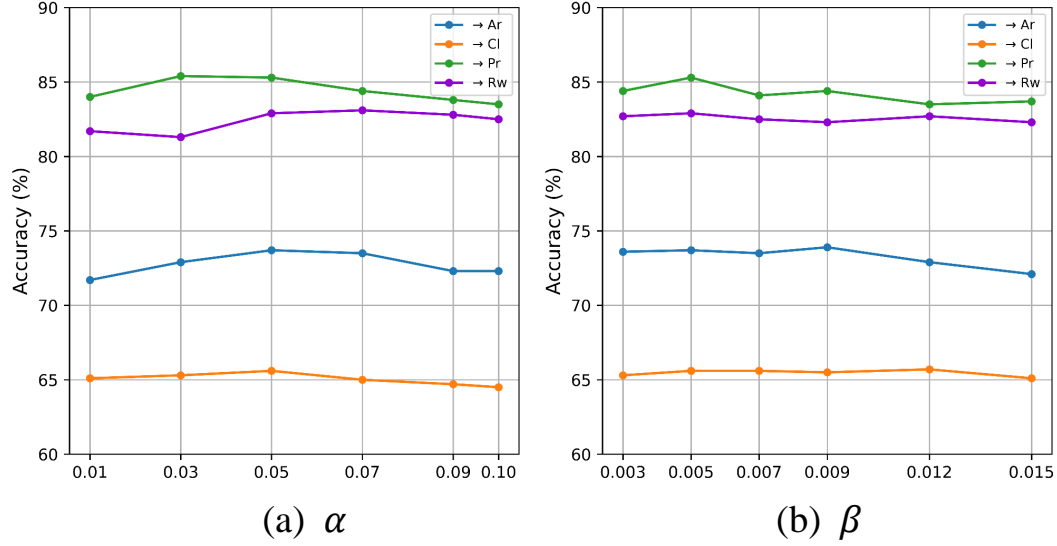


Figure 7: Sensitivity analysis of α and β .

As can be seen, the value of the hyperparameter α is somewhat greater and the β is taken at an overall smaller value. This indicates that the domain style centroid is updated more vigorously and provides a gradient sufficient for the backpropagation of the network. Memory M, on the other hand, requires a slower update to maintain network robustness because it involves the pseudo-label generation.